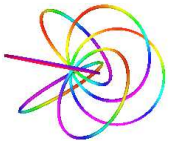

SYMCOMP 2015
Faro, March 26-27, 2015

NUMERICAL SIMULATION OF ELECTRICAL PROBLEMS IN A VACUUM DISJUNTOR

S. Clain[1] and J. Rodrigues [2]

1: Departamento de Matemática e Aplicações
Campus de Gualtar - 4710-057 Braga
e-mail: clain@math.uminho.pt

2:Área Departamental de Matemática
Instituto Superior de Engenharia de Lisboa
e-mail: jrodri@dec.isel.pt

Keywords: Finite element methods, Domain decomposition methods, Helmotz equations, Biot-Savard

Abstract. *A vacuum circuit breaker is a device that allows the cutting of electrical power. This device consists essentially of two electrodes, one of them being mobile and is subject to a mechanical force produced by a spring, giving rise to the contact between the two electrodes. The current passing between two electrodes is determined by the extension of the contact zone. Moreover, the passage of current generated Laplace forces in areas bordering the contact, but not yet in contact. Due to the curved geometry of the electrodes, these Laplace forces are opposite and therefore cause the repulsion of the electrodes. This means that for a given power we have to evaluate the electric potential, the magnetic field corresponding to the contact zone. bbm*

1 INTRODUCTION

A vacuum circuit breaker is a device that allows the cutting of electrical power. We refer figure 1 to showing the main parts of a typical vacuum interrupter. The apparatus core is essentially constituted of two electrodes, one of them being fixed (1) and the other one is mobile (3) and subject to a mechanical force produced by a spring, maintaining the contact between the two electrodes (2). The current passing between two electrodes is determined by the extension of the contact zone and generated Laplace forces in areas bordering the contact, but not yet in contact. Due to the curved geometry of the electrodes, Laplace forces are opposite and cause the repulsion of the electrodes. When the intensity reach a critical value, the forces separate the two electrodes and the circuit is breaking. For a given intensity and a contact length, we wish evaluate the repulsive Laplace force deriving from the electric and magnetic fields.

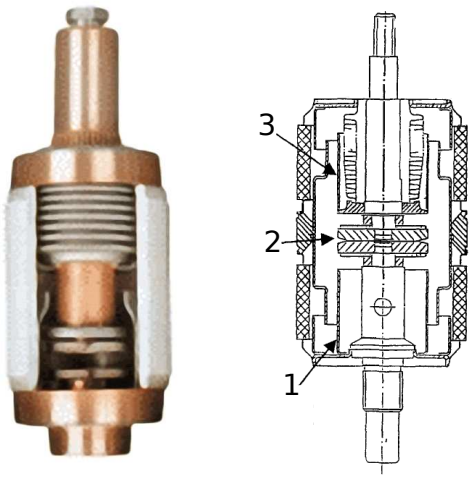

Figure 1: The circuit-breaker [1]

2 THE ELECTRICAL PROBLEM

2.1 Domain definition

At initial stage domain $\Omega = \Omega^a \cup \Omega^b$ corresponds to the initial situation where no force acts. Applying the gravity and the spring we get a displacement $\boldsymbol{u}$ over Ω and a new configuration characterized by an effective contact area $\mathcal{A}$ between the two subdomains. Due to the displacement $\boldsymbol{u}$, domain Ω is mapped into a new domain denoted $\widetilde{\Omega} = \widetilde{\Omega}(\boldsymbol{u}) = \widetilde{\Omega}^a(\boldsymbol{u}) \cup \widetilde{\Omega}^b(\boldsymbol{u})$ depending on the displacement field. In the same way, on has domains $\widetilde{\Omega}^\ell$, $\widetilde{\Gamma}^\ell_L$, $\widetilde{\Gamma}^\ell_C$, $\ell = a, b$ as well as $\widetilde{\Gamma}_B$ and $\widetilde{\Gamma}_U$. For the sake of simplicity, we shall use the

same notations $\boldsymbol{n}$, $\boldsymbol{t}$ to denote the outward normal vector and the tangential vector on the boundary. Notice that $\mathcal{A} = \widetilde{\Gamma}_C^a \cap \widetilde{\Gamma}_C^b$.
When the circuit breaker is close (the electrodes are in contact with a common area $\mathcal{A}$), the current flows across the interface governing by two main principles: conservation of the normal density current and a null potential jump across the interface, as represented at Figure 2 (a). Moreover, the electric current generate a Laplace force (as represented at Figure 2 (b)), repulsive at contact zone, which plays the fundamental role of a circuit breaker mechanism. When current increases, the Laplace force increases and the geometrical design of the apparatus results to a reduction of the contact surface till we reach a complete separation. The present chapter is dedicated to the construction of the electrical model where one computes the electric and the magnetic field in function of the contact surface.

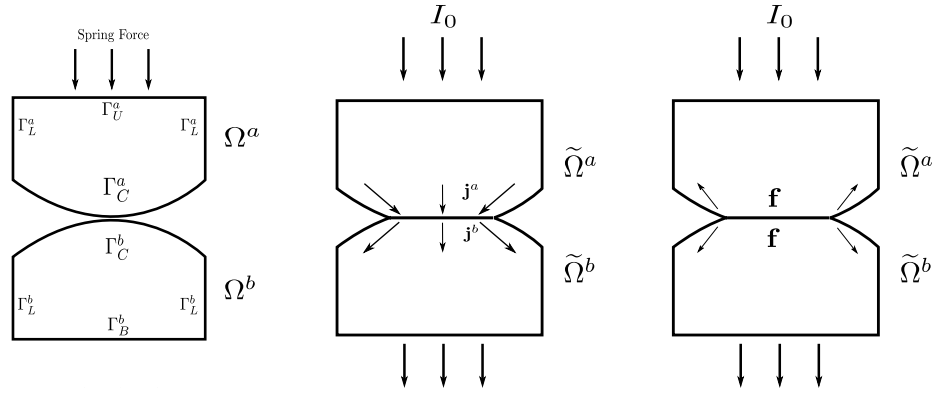

(a) The initial configuration

(b) The normal density current jump across the interface

(c) Global defined Laplace force

Figure 2: Electric-Magnetic problem outline

2.2 Mathematical modelling

A medium voltage circuit breaker is designed to work with continuous or low frequency current (for instance 50 Hz). It results that a common approach use the low frequency approximation (see Rappaz and Touzani [2]) where we neglect the displacement current and the induction effect. Consequently, we use the standard scalar potential formulation and denote by ϕ the scalar electrical potential while $\mathbf{E} = -\nabla\phi$ stands for the electric field and $\mathbf{j} = \sigma E$ represents the current density with $\sigma > 0$ the conductivity we suppose to be constant for the sake of simplicity. When necessary, we shall use the notations ϕ^ℓ, $\mathbf{E}^\ell$, $\mathbf{j}^\ell$, $\ell = a, b$ to characterise the quantities associated to domain $\widetilde{\Omega}^\ell$ respectively. Moreover component of the global vector writes $\mathbf{j} = \left(\mathbf{j}^a, \mathbf{j}^b\right) = \left((j_1^a, j_2^a,), \left(j_1^b, j_2^b, \right)\right)$, $\mathbf{E} = \left(\mathbf{E}^a, \mathbf{E}^b\right)$

and $\phi = \left(\phi^a, \phi^b\right)$.
Assuming that no electrical charge are present in the domain, the density current conservation writes

$$\nabla \cdot \mathbf{j} = 0, \text{ in } \widetilde{\Omega} \tag{1}$$

and deduce the scalar electrical potential formulation

$$-\nabla \cdot (\sigma \nabla \phi) = 0, \text{ in } \widetilde{\Omega} \tag{2}$$

We equipped the equation with the following boundary conditions: $\phi = 0$ on the basement $\widetilde{\Gamma}_B$, a uniform distribution on the upper side

$$\mathbf{j} \cdot \boldsymbol{n} = \frac{I_0}{|\widetilde{\Gamma}_U|} \tag{3}$$

with I_0 the intensity current while we prescribe an homogeneous Neumann condition for the rest of the boundary to model that fact that no current crosses the boundary which are in contact with the vacuum.

2.3 The two domains formulation

From a practical point of view, the electrical problem will be seen as the coupling of two subproblems defined in each subdomain. Here classical Sobolev spaces are used to obtain a variational formulation. We rewrite equation (2) in the following way: find ϕ^a and ϕ^b such that

$$-\nabla \cdot (\sigma \nabla \phi^\ell) = 0, \text{ in } \widetilde{\Omega}^\ell \tag{4}$$

with $\phi^b = 0$ on the basement $\widetilde{\Gamma}_B$, $\quad \mathbf{j}^a \cdot \boldsymbol{n}^a = \dfrac{I_0}{|\widetilde{\Gamma}_U|}$ while we assume homogeneous Neumann condition condition for the vacuum boundary. To complete the new model, we prescribe continuity for the normal current and potential across the contact zone:

$$\mathbf{j}^a \cdot \boldsymbol{n}^a + \mathbf{j}^b \cdot \boldsymbol{n}^b = 0, \qquad \phi^a = \phi^b, \qquad \text{on } \mathcal{A}. \tag{5}$$

Indeed, assume that $\phi \in H^1(\widetilde{\Omega}) \cap C^0(\widetilde{\Omega})$ is a solution of the one domain problem then from the continuity we deduce $\phi^a = \phi^b$ on $\mathcal{A}$. On the other hand, let $\psi \in H_0^1(\widetilde{\Omega})$, integration by part yields

$$0 = \int_{\widetilde{\Omega}} \sigma \nabla \phi \nabla \psi \, dx = \int_{\widetilde{\Omega}^a} \sigma \nabla \phi \nabla \psi \, dx + \int_{\widetilde{\Omega}^b} \sigma \nabla \phi \nabla \psi \, dx$$

Now, integration by parts on each subdomains provide

$$0 = \int_{\widetilde{\Omega}^a} -\nabla \cdot (\sigma \nabla \phi) \psi \, dx + \int_{\widetilde{\Omega}^b} -\nabla \cdot (\sigma \nabla \phi) \psi \, dx + \int_{\mathcal{A}} \sigma (\mathbf{j}^a \cdot \boldsymbol{n}^a + \mathbf{j}^b \cdot \boldsymbol{n}^b) \psi ds.$$

Relation (4) yields that for any $\psi \in H_0^1(\widetilde{\Omega})$ we have

$$\int_{\mathcal{A}} \sigma(\mathbf{j}^a \cdot \boldsymbol{n}^a + \mathbf{j}^b \cdot \boldsymbol{n}^b)\psi ds = 0$$

which implies

$$\mathbf{j}^a \cdot \boldsymbol{n}^a + \mathbf{j}^b \cdot \boldsymbol{n}^b = 0$$

.

3 THE MAGNETICAL FIELD

With $\mathbf{E}$ in hand, we deduce the current density $\mathbf{j}$ and we aim to compute the associated electrical field to at last deduce the Laplace force. To this end, let us by $\mathbf{B}$ the magnetic induction field. For three-dimensional configuration, the Ampère-Maxwell law writes

$$\nabla \times \mathbf{B} = \mu_0 \mathbf{j}, \quad \text{in } \mathbb{R}^3 \tag{6}$$

with μ_0 the magnetic permeability in the vacuum or non-ferromagnetic material.
Assuming invariance following the z direction and that the magnetic field only depend on x and y, we deduce that the only non-vanishing component is $B(x_1.x_2) = \mathbf{B}_z(x_1, x_2)$ and the Ampère-Maxwell equation writes

$$\partial_2 B = \mu_0 \mathbf{j}_1, \qquad -\partial_1 B = \mu_0 \mathbf{j}_2, \quad \text{in } \mathbb{R}^2$$

where $\mathbf{j}$ is a given function on $\mathbb{R}^2$ with compact support.
Dealing with the rotational operator $\nabla\times$ in $\mathbb{R}^2$, we deduce that B is also the solution of problem $\mu_0 \nabla \times \mathbf{j} = \nabla \times \nabla \times B = -\Delta B$ (see [2]) with the asymptotic behaviour $B(\boldsymbol{x}) = \mathcal{O}(|\boldsymbol{x}|^{-1})$ when $|\boldsymbol{x}| \to \infty$.
Another alternative is to introduce the potential magnetic vector $\mathbf{A}$ such that $B = \nabla \times \mathbf{A}$ where $\mathbf{A}$ is the solution of problem

$$\nabla \times (\nabla \times \mathbf{A}) = -\Delta \mathbf{A} = \mu_0 \mathbf{j}, \quad \text{in } \mathbb{R}^2$$

with the asymptotic behaviour $|\mathbf{A}(\boldsymbol{x})| = \mathcal{O}\big(\ln(|\boldsymbol{x}|)\big)$.
However this relationship is not useful for magnetic field computation since the function is defined in the whole domain $\mathbb{R}^2$ while we just need to determine B on domain $\widetilde{\Omega}$. An alternative approach consists to use the integral representation, namely the Biot-Savart formula. For two-dimensional geometries $\widetilde{\Omega} \subset \mathbb{R}^2$ (see [3]). The vector potential magnetic field and the magnetic field at a point $\boldsymbol{x}$ are given by

$$\mathbf{A}(\boldsymbol{x}) = -\frac{\mu_0}{2\pi} \int_{\widetilde{\Omega}} \mathbf{j}(\boldsymbol{y}) \ln(|\boldsymbol{x} - \boldsymbol{y}|) d\boldsymbol{y} \tag{7}$$

$$B(\boldsymbol{x}) = \nabla_{\boldsymbol{x}} \times \mathbf{A} = -\frac{\mu_0}{2\pi} \int_{\widetilde{\Omega}} \mathbf{j}(\boldsymbol{y}) \times \nabla_{\boldsymbol{x}} \ln(|\boldsymbol{x} - \boldsymbol{y}|) d\boldsymbol{y}, \tag{8}$$

for a current $\mathbf{j}$ flowing in the direction of $\mathbf{e}_1$ and $\mathbf{e}_2$ where $\times$ represents the external product between two vectors. After some algebraic manipulation, equation (8) writes

$$B(\boldsymbol{x}) = \frac{\mu_0}{2\pi}\int_{\widetilde{\Omega}} \frac{\det[\mathbf{j}(\boldsymbol{y}),(\boldsymbol{x}-\boldsymbol{y})]}{|\boldsymbol{x}-\boldsymbol{y}|^2} d\boldsymbol{y}. \tag{9}$$

At least, the Laplace force is given by

$$\mathbf{f} = \mathbf{j} \times \mathbf{B},$$

and in our specific case with $\mathbf{B} = B\mathbf{e}_3$, the force writes

$$\begin{pmatrix} f_1 \\ f_2 \end{pmatrix} = B \begin{pmatrix} j_2 \\ -j_1 \end{pmatrix}. \tag{10}$$

4 MATRICIAL REPRESENTATION

4.1 Representation for $A^a_{e_h}$

Using finite element methods we will introduce the matricial representation for this problem. We identify the new meshes of $\widetilde{\Omega}^\ell$ by $\widetilde{\mathcal{T}}^\ell_h$, $\ell = a, b$, respectively, and To enforce the Dirichlet condition we use a penalisation method which seems more adapted. Indeed, the contact zone may change with respect to the elasticity problem hence to avoid a new codification of the boundary and to reshape the matrix, we always use the same stiff matrix and introduce the Dirichlet condition by multiplying the entries corresponding to the nodes of $\mathcal{A}^a_{\eta,h}$.

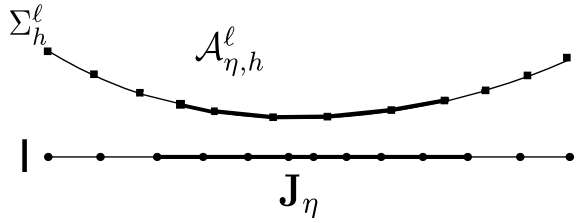

Figure 3: Discrete active zone definition

The rigid matrix writes

$$[A^a_e] = \left[A^a_{e_h}\left(\phi^a_i, \phi^a_j\right)\right]_{i,j=1,\ldots,n^a}$$

while the associated write-hand side is given by

$$[\Theta^a]_i = \begin{cases} 0 & \Leftarrow \quad i \in \{1,\ldots,\tilde{n}^a\} \\ \int_{\widetilde{\Gamma}_{U_h}} \frac{I_0}{|\widetilde{\Gamma}_{U_h}|}\varphi^a_i \, ds, & \Leftarrow \quad i \in \{\tilde{n}^a+1,\ldots,n^a\} \end{cases}$$

Let denote by $\mathcal{E}^a_{\eta,h}$ the nodes which correspond to domain $\mathcal{A}^a_{\eta_h}$. Once we compute the system matrices at each step, the Dirichlet condition correspondent to $\mathcal{A}^a_{\eta_h}$ can be imposed by substitution method.
Resolution of the elliptic problem turns to solve the simple matricial problem

$$[A^a_e]\,[\Phi^a] = [\Theta^a]$$

where $[\Phi^a]$ are the unknowns on the nodes.

4.2 Representation for $A^b_{e_h}$

Since the Dirichlet condition does not change with the iteration, we do not use a penalization method for operator $A^b_{e_h}$ and recall that P_i, $i = 1, \cdots, \tilde{n}^b$, correspond to the nodes of $\widetilde{\Omega}^b$ except the node of boundary $\widetilde{\Gamma}_B$. The rigid matrix then writes

$$\left[A^b_e\right] \;=\; \left[A^b_{e_h}\left(\phi^b_i, \phi^b_j\right)\right]_{i,j=1,\ldots,\tilde{n}^b}$$

Let ρ^b_h be a given constant piecewise function on $\widetilde{\Gamma}^a_{C_h}$ characterized by vector $[\rho] = \left[\rho_1 \cdots \omega_{s^b_C}\right]^T$. We introduce the Neumann conditions with vector

$$\left[\Theta^b\left([\rho]\right)\right]_i = \sum_{T \subset \widetilde{\Gamma}^b_{C_h}} \int_T \rho^b_h \phi^b_i \, ds, \Leftarrow i \in \left\{1, \ldots, n^b_C\right\}.$$

The elliptic problem consist in solving the matricial problem

$$\left[A^b_e\right]\left[\widetilde{\Phi}^b\right] = \left[\Theta^b\right]$$

where $\left[\widetilde{\Phi}^b\right]$ are the unknowns on the nodes. We complete the vector setting $\left[\Phi^b\right] = \left[\left[\widetilde{\Phi}^b\right], 0\right]$ taking into account the homogeneous boundary condition.

4.3 Current density and normal projection

Setting $\mathbf{j}^\ell_h = \nabla\phi^\ell_h \in X^\ell_h$, we obtain a constant piecewise vector over $\widetilde{\Omega}^\ell_h$ which represents the current density field. We shall represent the vector in two vectors depending on the coordinates,

$$\left[\mathbf{j}^\ell_1\right] \;=\; \left[\; \mathbf{j}^\ell_{1,1} \cdots \mathbf{j}^\ell_{n^\ell_K,1} \;\right]^T \;\text{ and }\; \left[\mathbf{j}^\ell_2\right] \;=\; \left[\; \mathbf{j}^a_{1,2} \cdots \mathbf{j}^a_{n^\ell_K,2} \;\right]^T.$$

that we gather in the matrix form

$$\left[\,\mathbf{j}^\ell\,\right] \;=\; \left[\;\left[\mathbf{j}^\ell_1\right] \;\; \left[\mathbf{j}^\ell_2\right]\;\right]^T.$$

We report here the definition of the matricial expression of the projection following the normal direction. We denote by $\left[\overline{N}^{\ell}\right] \in \mathbb{R}^{n_C^{\ell} \times 2n_C^{\ell}}$ the matrix of the outwards normals over Γ_C^{ℓ} and set

$$\left[\overline{N}^{\ell}\right] = \begin{bmatrix} \boldsymbol{n}_{h\,1,1}^{\ell} & \cdots & 0 & \boldsymbol{n}_{h1,2}^{\ell} & \cdots & 0 \\ & \ddots & & & \ddots & \\ 0 & \cdots & \boldsymbol{n}_{h\ n_C^{\ell},1}^{\ell} & 0 & \cdots & \boldsymbol{n}_{h\ n_C^{\ell},2}^{\ell} \end{bmatrix}$$

We introduce the global matricial representation of $\left[\overline{N}^{\ell}\right]$ on Ω_h^{ℓ}:

$$\left[N^{\ell}\right] = \begin{bmatrix} \left[\overline{N}^{\ell}\right] & \mathbf{0} \end{bmatrix}$$

with $[N^a] \in \mathbb{R}^{n_C^{\ell} \times (\tilde{n}^a + n^a)}$ and $\left[N^b\right] \in \mathbb{R}^{n_C^{\ell} \times 2\tilde{n}^b}$.

4.4 Representation for the mappings on contact zone

We recall the matricial representation $\left[C^{\ell,I}\right] \in \mathbb{R}^{n^I \times n_C^{\ell}}$ and $\left[C^{I,\ell}\right] = \left[C^{\ell,I}\right]^T \in \mathbb{R}^{n_C^{\ell} \times n^I}$ for operators $C_{h,\eta}^{\ell,I}$ and $C_{\eta,h}^{I,\ell}$ respectively

$$\left[C^{\ell,I}\right]_{ki} = \int_I \mu_k(\xi)\phi_i^{\ell}(\xi)d\xi, \quad k = 1, \cdots, n^I,\ i = 1, \cdots, n_C^{\ell}.$$

In the same way, we represent operators $D_{h,\eta}^{\ell,I}$ and $D_{\eta,h}^{I,\ell}$ with $\left[D^{\ell,I}\right] \in \mathbb{R}^{s^I \times s_C^{\ell}}$ and $\left[D^{I,\ell}\right] = \left[D^{\ell,I}\right]^T \in \mathbb{R}^{s_C^{\ell} \times s^I}$ with

$$\left[D^{\ell,I}\right]_{ki} = \int_I \lambda_k(\xi)\vartheta_i^{\ell}(\xi)d\xi, \quad k = 1, \cdots, s^I,\ i = 1, \cdots, s_C^{\ell}.$$

4.5 The iterative problem within the matricial form

We now give the iterative procedure at the matricial level. Notice that the procedure corresponds to the one one really implemented on computer thus the importance to define completely all the step. The iterator index is r and we shall compute a sequence of vectors $[\nu]^r$ which shall converge.
Assume that vector $[\nu]^r$ is known such that $[\nu]_k^r = 0$ for the nodes N_k outside of $\mathbf{J}_{\eta}$. the procedure is given by the following substeps (we omit subscript k for the sake of simplicity):

1. Compute vector $[w^a] = \left[D^{I,\ell}\right][\nu]^r$
2. Compute $[\Phi^a]$ solving problem

$$[A_e^a][\Phi^a] = [\Theta^a]$$

with penalization with respect to $[\omega^a]$.

3. Compute $[\mathbf{j}^a]$ with $\nabla\phi_h^a$ and compute $[\rho^a] = [N^a][\mathbf{j}^a]$.
4. Compute $[\tau] = \left[D^{\ell,I}\right][\rho^a]$ and $[\rho^b] = -\left[D^{\ell,I}\right][\tau]$
5. Compute $\left[\Phi^b\right] = \left[\left[\widetilde{\Phi}^b\right], 0\right]$ solving

$$\left[A_e^b\right]\left[\widetilde{\Phi}^b\right] = \left[\Theta^b\right]$$

6. Extract $[\omega^b]$ from $\left[\Phi^b\right]$ and compute $[\tilde{\nu}] = \left[C^{\ell,I}\right][\omega^b]$ where we cancel the entries k which correspond to the nodes N_k outside of $\mathbf{J}_\eta$.
7. Compute the new vector $[\nu]^{r+1} = \theta[\nu]^r + (1-\theta)[\tilde{\nu}]$

We repeat the algorithm till we satisfy the convergence criterion.

5 NUMERICAL SIMULATION

5.1 One domain case

We begin by considering the case with one domain. Once the length of $\mathbf{J}_\eta$ is determined we solve the discrete electric problem on the domain have the configuration of the two electrodes in contact, Figure 4. We this domain we do not have to worry about the potential continuity at the contact zone. More, these results will give us a benchmark for the later results obtained with the domain decomposition technique and two domains.
For this case we consider $m(\mathbf{J}_\eta) = 0.0468$ and $I_0 = 10kA$.

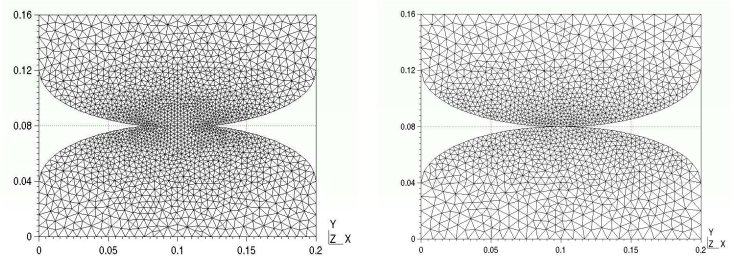

(a) One domain mesh (b) Two domain meshes

Figure 4: Domain mesh

Figure 4 shows that with both strategies we obtain very similar results. This validates the results and in particular our technique for passing information between the domains at domain decomposition method.
At Figures 6 and 7 although the range of values are similar, the observed difference is justified by the mesh difference, since the density is approximated numerically in the

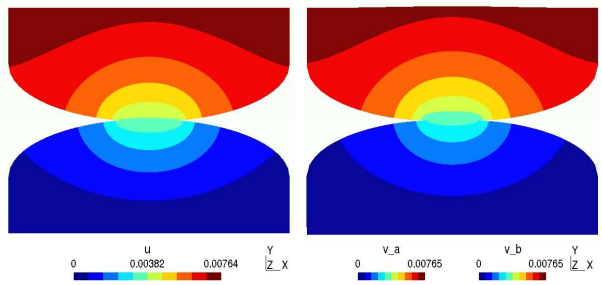

(a) One domain (b) Two domains

Figure 5: Potential scalar field

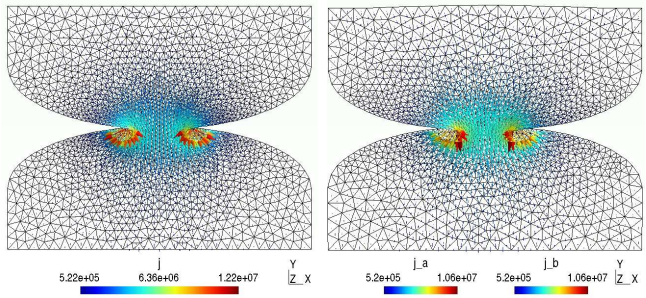

(a) One domain (b) Two domains

Figure 6: Current density field

barycentric coordinates in the element from the given potential at the nodes. Also in these figures we can see the continuity of density at the the contact zone.
The magnetic induction (component following $\mathbf{e}_3$) is exactly the same Figure 8. About Laplace force there is a reduction though the magnitude is equal and we have almost the symmetry between the two domains Figure 9, where we recall again that the meshes are not symmetrical and that the Laplace force are calculated is approximated numerically in the barycentric coordinates in the element.
At this section we will analyse the numerical solutions produced at electro-magnetic state when the electrodes are in contact through a determined active zone.
For each numerical problem we determine the volume repulsive force generated for a given $m(\mathbf{J})$ and intensity current I_0, for two profiles cases: elliptic and circular.

5.2 Two domains case

We are interested to analysing the profiles of the potential contact zone: elliptic and circular. From [4] we use two intensity values $I = 10$ kA , $I = 20$ kA, $I = 40$ kA and

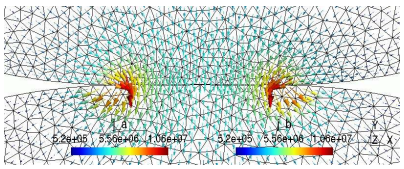

Figure 7: Zoom of current density field at contact zone

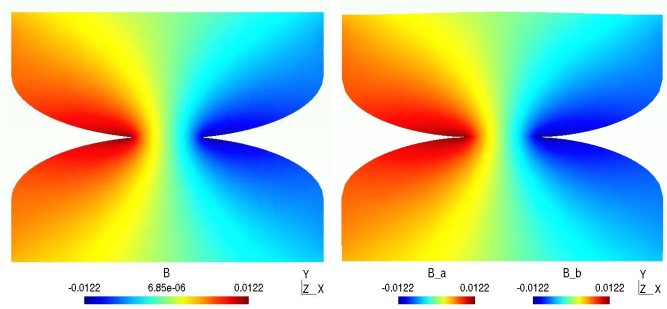

(a) One domain (b) Two domains

Figure 8: Magnetic induction (component following $\mathbf{e}_3$)

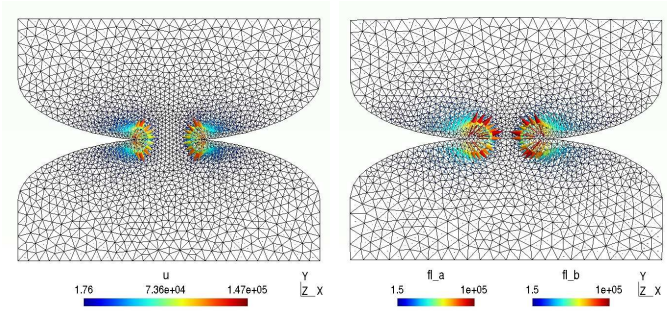

(a) One domain (b) Two domains

Figure 9: Laplace force

$I = 60$ kA. We consider that a inicial spring force has applied, characterized by

$$F = \kappa \times \alpha \ (N) \tag{11}$$

with

$$\kappa = \frac{E \times A}{L} \tag{12}$$

named the axial stiffness, where
$E = 115$ GPa $= 115 \times 10^6 \mathrm{N/m^2}$, the copper elasticity modulus, [5],

A, the contact zone area (in m^2) and
L the circuit breaker height (in m).
The value α represents the vertical displacement, so here we will suppose $\alpha \leq 0.2$

5.3 Elliptic profile

Here we consider a contact with a elliptic profile with a contact zone length $m(\mathbf{J}_\eta) = 0.032$, corresponding to $\alpha = 0.1$.

Table 1: Repulsive force generated with an elliptic profile and large active zone and test for several values of θ

intensity current (A)	θ	repulsive force generated (N)
1×10^4	.125	44.53
1×10^4	.25	44.53
1×10^4	.5	44.53
2×10^4	.125	178.13
2×10^4	.25	178.13
2×10^4	.5	178.13
4×10^4	.125	712.53
4×10^4	.25	712.53
4×10^4	.5	712.53
6×10^4	.125	1603.2
6×10^4	.25	1603.2
6×10^4	.5	1603.2

From the results explained at Table 1, we can expect a function of the kind

$$f_R(I_0) = a_1 I_0^2. \tag{13}$$

Using least squares method we obtain

$$a_1 = 44.53.$$

represented at Figure 10.

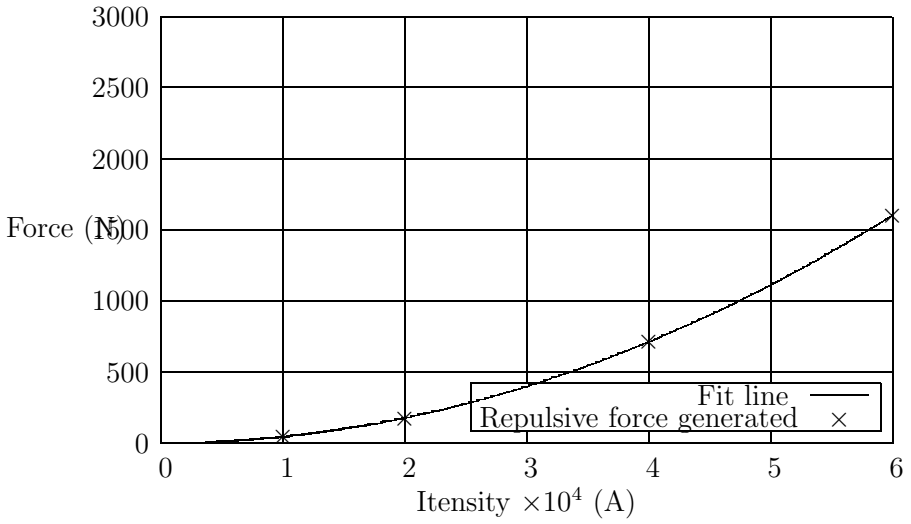

Figure 10: Elliptic profile and large active zone: Repulsive force generated "×" and least squares approximation "line"

Now we test a reduction of the contact zone, $m(\mathbf{J}_\eta) = 0.012$, corresponding to $\alpha = 0.01$.

Table 2: Repulsive force generated with an elliptic profile and small active zone

intensity current (A)	repulsive force generated (N)
1×10^4	51.1
2×10^4	204.42
4×10^4	817.69
6×10^4	1839.82

From the results explained at Table 2, we can expect a function of the kind

$$f_R(I_0) = a_2 I_0^2. \tag{14}$$

Using least squares method we obtain

$$a_2 = 51.1.$$

represented at Figure 11.

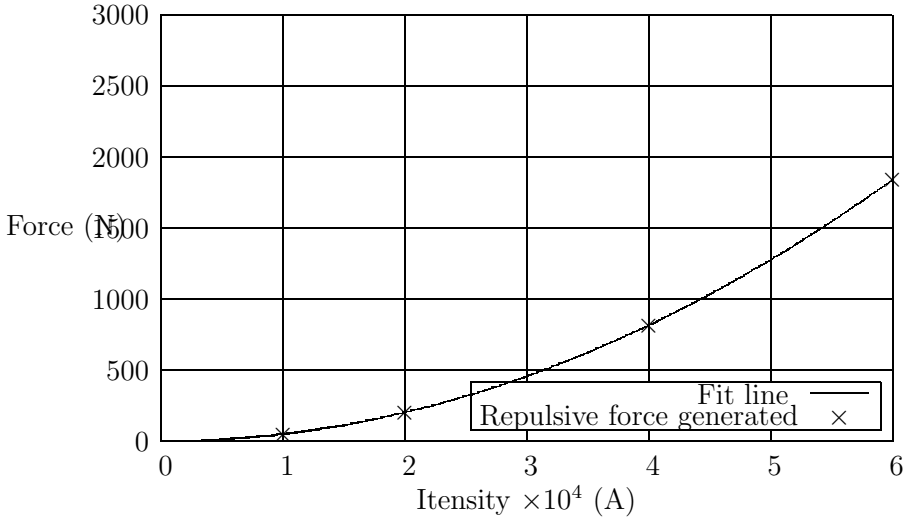

Figure 11: Elliptic profile and small active zone: Repulsive force generated "×" and least squares approximation "line"

6 Circular profile

Here we begin by consider a circular contact profile after deformation with$m(\mathbf{J}_\eta) = 0.045$, corresponding to $\alpha = 0.1$.
From the results explained at Table 3, we can expect a function of the kind

$$f_R(I_0) = a_3 I_0^2. \tag{15}$$

Using least squares method we obtain

$$a_3 = 186.71.$$

represented at Figure 12.
Like as above Consider now a small contact zone, $m(\mathbf{J}_\eta) = 0.016$, corresponding to $\alpha = 0.01$.
From the results explained at Table 4, we can expect a function of the kind

$$f_R(I_0) = a_4 I_0^2. \tag{16}$$

Table 3: Repulsive force generated with an circular profile and large active zone

intensity current (A)	repulsive force generated (N)
1×10^4	186.71
2×10^4	746.85
4×10^4	2987.42
6×10^4	6721.69

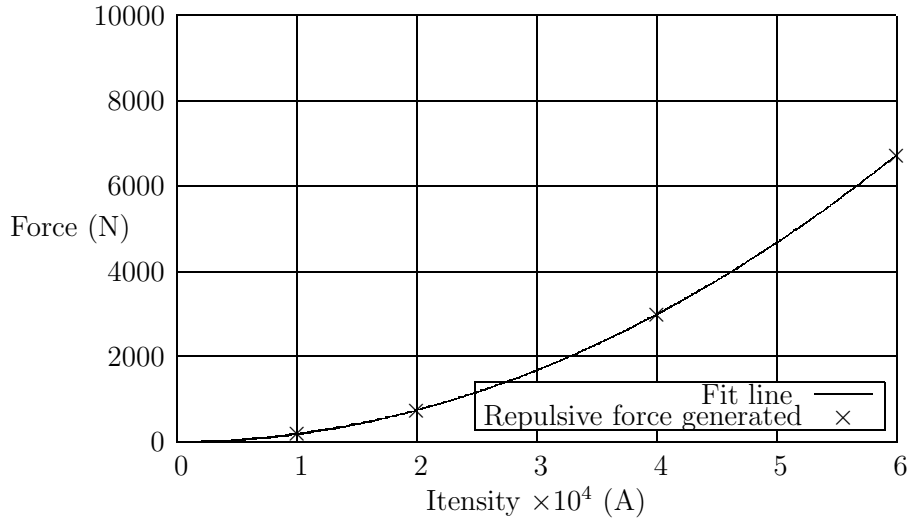

Figure 12: Circular profile and large active zone: Repulsive force generated "×" and least squares approximation "line"

Using least squares method we obtain

$$a_4 = 200.35.$$

represented at Figure 13.
Observing figures we note that the repulsive force depends on the electrode profile being more important in the case of a circular profile. It also appears that the repulsive force increases as the extent of the active area decreases.

Table 4: Repulsive force generated with an circular profile and small active zone

intensity current (A)	repulsive force generated (N)
1×10^4	200.34
2×10^4	801.39
4×10^4	3205.59
6×10^4	7212.59

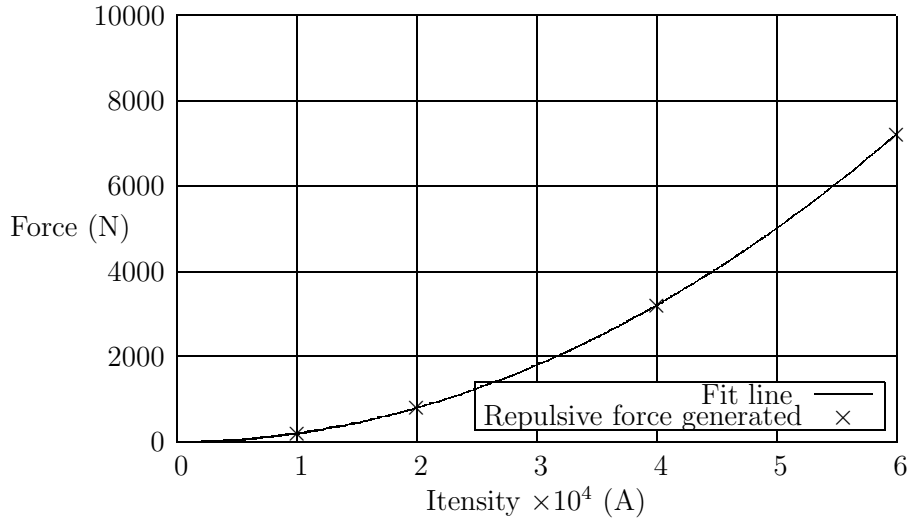

Figure 13: Circular profile and small active zone: Repulsive force generated "×" and least squares approximation "line"

7 CONCLUSION

From the results we have obtained can conclude that the proposed domain decomposition algorithm converges to a continuous solution of the scalar electrical potential field, independently of parameter θ.
Comparing figures 10 - 12 and 11 - 13 we note that the repulsive force depends on the electrode profile and being more important in the case of a circular profile.
With this tests, we can also observe that the repulsive force is inversely proportional to the length of the active zone.
Only two-dimensional configurations have been considered in the present work but the

real problem is three-dimensional and brings more difficulties. The contact zone is more complex and the computational effort is larger.

8 REFERENCES

[1] R. Garzon. *High Voltage Circuit Breakers: Design and Applications*. Pitman Advanced Publishing Program, Boston, 1985.

[2] J. Rappaz R. Touzani. *Mathematical Models for Eddy Currents and Magnetostatics With Selected Applications*. Springer - Scientific Computation, New-York, 2014.

[3] J.-C. Suh. The evaluation of the biot-savart integral. *Journal of Engineering Mathematics*, pages 375–395, 2000.

[4] A. Slama. *Modlisation des sources de courant en mouvement et des efforts lectrodynamiques dans les appareils de coupure*. PhD gnie electrique, Institut National Polytechnique de Grenoble - France, 2001.

[5] American Society for Metals Handbooks. Metals handbook, January 2012.